2024 IEEE/RSJ International Conference on Intelligent Robots and Systems (IROS)
October 14-18, 2024. Abu Dhabi, UAE

Development of a Super-thin and Fast Omnidirectional Treadmill through a Novel Helical Transmission Mechanism

Sanghun Pyo[1], Jinsun Choi[2], and Jungwon Yoon[2,] *, *Member, IEEE*

***Abstract*— To effectively enhance the spatial sensation for an immersive user experience (UX) in virtual reality (VR), the locomotion interface (LI) is one of the most critical factors. To offer a room-scale LI suitable for use in typical office or home environments, it is imperative that the LI device enables a natural walking experience while occupying minimal space. To realize LI for all directions, an omnidirectional treadmill (ODT) can successfully achieve 2-dimensional holonomic motion (X and Y axes) and provide the most natural walking experience, such as walking on real ground. However, a problem arises due to the excessive system thickness caused by the torus structure of a large treadmill (X-axis) carrying several small treadmills (Y-axis), along with the installation of a complex power transmission mechanism inside the ODT. To reduce the thickness of its double-layer and complex structure, we propose an ODT with a novel transmission mechanism. The proposed ODT utilizes helical timing pulleys (HTPs) to generate Y-axis motion and helical gears (HGs) to synchronized-actuate the HTPs. As a result, the proposed ODT achieves a super-thin configuration and fast actuation performance. A pilot test of the proposed ODT was conducted to assess its maximum performance. The results indicate achievable speeds of 3.175 m/s and 4 m/s, along with an acceleration of 5 m/s² for both the X and Y axes, respectively.**

I. Introduction

With the development of virtual reality (VR) technology, various industries widely utilize VR-related products to improve the situation response-ability for training, safe rehabilitation, low-cost design, and productivity by providing diverse VR scenarios [1]. However, the progress of the VR industry has been hindered by factors such as the high cost of VR interactive equipment, a shortage of diverse content, and limited immersion of user experience (UX) [2][3].

To solve the slow spread of VR technology, the locomotion interface (LI) is considered one of the appropriate solutions to enhance UX immersion [4-6]. LI is achieved through a device that allows users to physically walk while remaining in a stationary position, aided by a controller that maintains the user in the reference position by predicting an intentional walking speed [7]. It can provide users with a more realistic environmental interaction by simulating walking, incorporating metabolic energy consumption and the sense of space generated by visual feedback, all while maintaining the user's position stationary when a user is dynamically walking [8][9]. Especially, an omnidirectional LI platform simulating the 2-dimensional ground effectively enhances immersion and engagement in VR applications such as soldier training, FPS games, architectural designs, virtual trips, rehabilitation programs, and more, resulting in a more attractive UX [10].

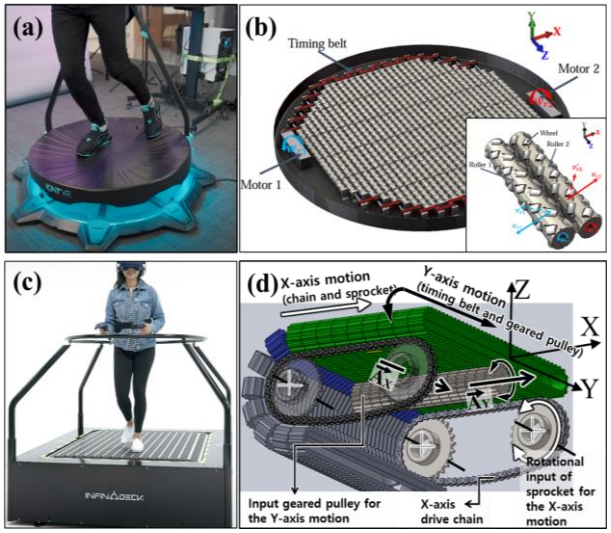

Figure 1. Three types of schemes for constructing of an omnidirectional locomotion interface (LI) - (a) sliding type with a low friction plate [11][12], (b) 45-degree wheel-based type[14][15], (c) and (d) omnidirectional treadmill (ODT) type [20][21].

Figure 1 summarizes representative schemes for composing an omnidirectional Locomotion Interface (LI) platform, including commercially available products or those capable of holonomic generation of the infinity 2-dimensional ground. The sliding type using a low friction surface is shown in Figure 1(a). [11][12]. The user's waist is tied to the machine. The user must either wear a pair of roller shoes or step onto a specialized low-friction surface. The primary issue with this LI type is the significant effort required to overcome the friction, making it challenging to simulate backward or lateral movements [13]. As a result, users cannot move with a natural walking pattern.

Another scheme is the 45-degree wheel-based scheme [14][15], as shown in Figure 1(b). To create a holonomic 2D ground, the main concept of using this method is inspired by the kinematics of a Mecanum wheel robot [16]. This type can compose LI platform the much thinner than the omnidirectional treadmill (ODT) type shown in Figure 1(c) and (d). Thus, it may be suitable for use as a room-scale LI due to the advantage of being thin. However, it provides a different sensation from actual ground due to the passive wheel rotation during walking in this system and does not naturally interface with a user's fast movements.

[1]Sanghun Pyo is with the Center for Nanorobotics in Brain, Gwangju Institute of Science and Technology (GIST), 123 Cheomdan-gwagiro, Buk-gu, Gwangju 61005, Korea (e-mail:pyopyo83@gm.gist.ac.kr)

[2]Jinsun Choi and Jungwon Yoon are with the Integrated Institute of Technology, Gwangju Institute of Science and Technology (GIST), 123 Cheomdan-gwagiro, Buk-gu, Gwangju 61005, Korea (e-mail: lunacloud611@gm.gist.ac.kr, jyoon@gist.ac.kr).

* Corresponding author

Figures 1(c) and (d) illustrate the ODT type as the representative omnidirectional LI platform, constructed by extending a belt-based treadmill into 2 dimensions. As a result, it has the torus structure as a large treadmill (X-axis) carrying numerous small treadmills (Y-axis). This scheme has been applied in several previous works, such as the Torus [17], Cyberwalk [18], and US Army ODT [19]. The commercialized product called Infinadeck is also based on this scheme, as shown in Figure 1(c) [20]. The ODT type can not only generate a holonomic 2D infinite ground through its torus structure but also deliver an experience that is closest to the real ground compared to other types. However, the ODT-type systems mentioned above have limited motion performance for handling fast LIs due to low power transmission efficiency. To solve the transmission problems of existing ODT systems, the authors of this paper previously developed the fast-ODT based on gear transmission in 2018, as shown in Figure 1(d) [9]. At that time, it achieved the fastest motion performance among other ODTs, reaching speeds of up to 3 m/s with an acceleration of 3 m/s². Due to its highspeed and acceleration, we were able to interface the user's rotational running naturally [21].

However, as highlighted in [14][15], the major limitation of ODTs lies in the challenge of reducing their thickness because of their torus structure and the installation of a complex power transmission mechanism inside. To provide immersive VR services even in general environments (home or office), a LI platform must occupy a small physical space, achieve sufficient motion performance, and operate as quietly as possible. Fast and super-thin LI solutions are crucial technologies for further advancing the VR industry. In this paper, we introduce a fast and super-thin ODT using a novel helical transmission mechanism, aiming to combine the benefits of the slim thickness in the Mecanum-wheel scheme with the capability of the ODT type to simulate real ground.

Compared to the ODT developed by the authors [9][21], which utilizes a timing pulley-based spur gear-type transmission, the thickness has been reduced from 64 cm to 24 cm. Additionally, both the maximum speed and acceleration have improved, increasing from 3 m/s and 3 m/s² to 4 m/s and 5 m/s², respectively. Moreover, it may reduce noise because the helical transmission can transfer power much smoother than spur transmission.

The remainder of the paper is organized as follows: Section 2 presents the proposed novel design scheme for the ODT. Section 3 describes how to design the main components for composing the helical transmission in the proposed ODT. Section 4 presents experimental results to validate the novel helical transmission scheme and compares its performance with other ODT systems. Finally, Section 5 summarizes the results and explains the future work.

II. Conceptual Design

A. System overview and thinner power transmission design

Figure 2 conceptually illustrates the main components and the arrangement method for generating a 2D holonomic infinite ground through independent X and Y-axis operations in the proposed ODT. In Figure 2(a), the X-axis motion of the proposed ODT is generated by the X-axis motor driving the sprocket and the segment attached to the chain, which moves directly. As shown in Figure 2(b), a standard timing belt (STB) is installed around the segment structure, and the Y-axis motion of the proposed ODT is achieved by rotating the helical timing pulley (HTP) to drive the STB. The HTPs are arranged continuously at regular intervals to form the HTP array, as shown in Figure 2(a), and all the installed HTPs have their teeth aligned to create a collinear line, as shown in Figure 2(c). Once the collinear line is formed, the HTP array can drive the STB independently, enabling each motion (X-axis and Y-axis) to operate independently, even when the segment moves along the X-axis.

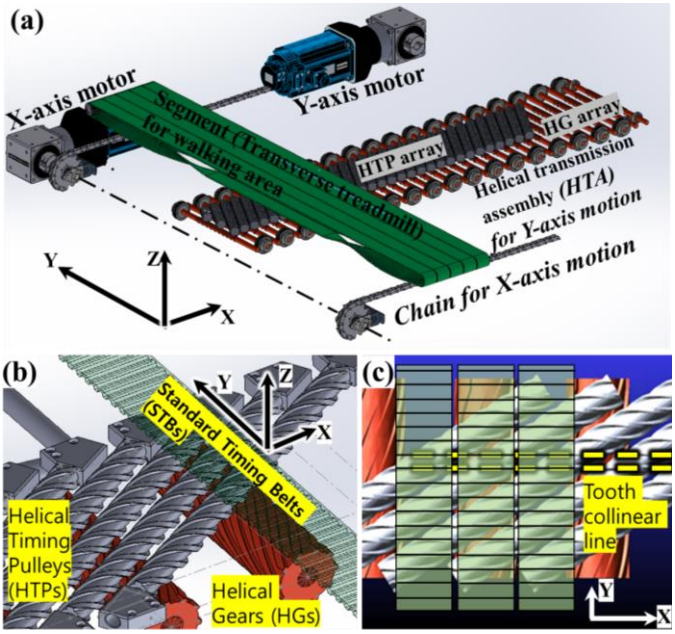

Figure 2. Schematic design of the proposed ODT's transmission system and generation of 2D holonomic infinite ground through independent X and Y-axis operation. (STB: Standard timing belt, HTP: Helical timing pulley, HG: Helical gear, HTA: Helical transmission assembly)

The HTP array is in direct contact with the STB teeth, which requires a tilted installation to drive a general timing belt (i.e., STB) using helical transmission. Furthermore, it is essential for all the STBs in the area where the user walks to operate simultaneously. Even during X-axis motion, it is necessary to maintain the tooth collinear line consistently to ensure stable power transmission for Y-axis motion. To mechanically achieve synchronized actuation of the tilted HTPs, the HTP array is driven by a helical gear (HG) array, as shown in Figure 2(a) and (b).

As shown in Figure 2(a), the most unique feature of the helical transmission assembly (HTA) used in the proposed ODT is that one HTP is driven by multiple HGs, and vice versa. Conceptually, when only one HG rotates, all HTPs and all HGs operate in unison, enabling mechanical synchronization of the HTPs to maintain the tooth collinear line. The driving mechanism for the STBs follows the same concept as the HTPs-HGs power transmission method, where multiple HTPs are arranged to drive a single STB. This HTA configuration offers a stable STB drive due to its high stiffness characteristics achieved by multiple tooth couplings.

As shown in Figure 3(a), the F-ODT utilizes an Omni-pulley system, which combines spur gear drive and Omni-

wheels, leading to enhanced STB operating efficiency through tooth-coupling-based transmission. Consequently, it achieved a motion performance of 3 m/s and an acceleration of 3 m/s², effectively enabling a stable omnidirectional human running interface [20]. However, to accommodate enough STB teeth, the use of a large-diameter component became necessary. This resulted in excessive thickness, rendering it unsuitable for a room-scale locomotion interface, with a thickness reaching 64 cm [21].

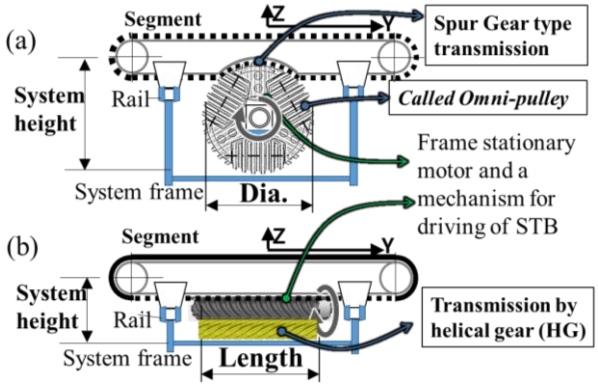

Figure 3. Comparison of power transmission mechanisms for Y-axis motion of (a) F-ODT and (b) the proposed ODT

As shown in Figure 3(b), the HTA used in the proposed ODT also employs tooth coupling with the STB, thereby enabling the achievement of a power transmission efficiency like that shown in Figure 3(a). Moreover, it became feasible to combine an adequate number of teeth with the STB belt by increasing the axial length of the transmission components (HTP, HG), rather than their diameter. This significant improvement allowed for a substantial reduction in the system's thickness by using smaller diameter HTP and HG.

B. A feature of the proposed system due to the tilted HTPs

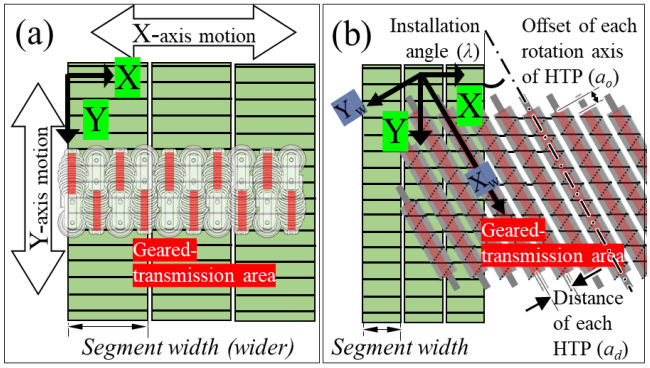

Figure 4. Comparison of changes in segment width due to differences in power transmission method (a) Omni-pulley, (b) HTP and HG

For an ODT to have a thin shape, it is necessary not only reduce to the size of an inside power transmission mechanism but also minimize to the width of the segments constituting the torus structure. This is because the segment can still rotate smoothly on the X-axis sprocket (See Figure 1) even when a reduced pitch diameter of the chain sprocket is applied. As shown in Figure 4(a), in the previous design of the F-ODT that utilized the Omni-pulley, the segment width had to be substantial to ensure stable tooth coupling between the STB and Omni-pulley. This was necessary due to the features of the Omni-pulley's discrete tooth coupling area (1 STB alternately driven by 2 tooth areas in 2 Omni-pulleys).

On the other hand, the proposed helical transmission mechanism creates a relatively continuous and wide power transmission area due to the array composed of the tilted HTPs, as shown in Figure 4(b). Thus, even though the segment width is extremely small, unlike the existing F-ODT, an HTP can connect to the teeth of multiple STBs (1 HTP driving 2 to3 STBs). In summary, the HTA consisting of HTP and HG with small-diameter shapes can combine a sufficient number of teeth for the stable operation of the STB. Moreover, due to the tilted HTP, it allows stable tooth coupling even when the segment width is reduced. As a result, it was possible to design the super-thin ODT.

III. Design Method of HTA Components (HTP, HG)

A. Design of the helical timing pulley (HTP) and HTP array

- *The condition of HTP-STB tooth coupling*

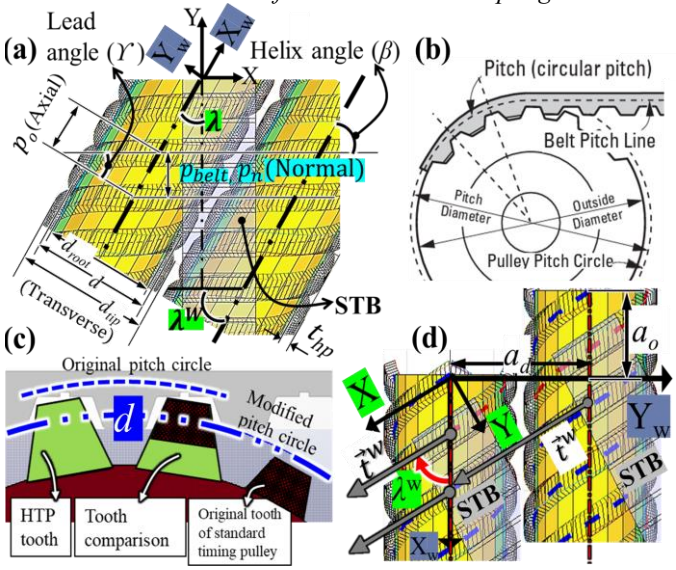

Figure 5. (a) HTP design parameters, (b) Standard timing pulley parameters and its pitch circle location, (c) Changing the pitch circle position by increasing the height of the tooth to enable gear transmission.

For STBs and HTPs to be mechanically combined for Y-axis motion, the axial pitch (p_o) and helix angle, β, of the HTP need to be set according to the STB pitch (p_{belt}) and the installation angle, λ, of the HTP, as shown in Figure 5(a). Obviously, even though the HTP installation angle is changing, the STB pitch and HTP normal pitch (p_n) must be the same for proper helical transmission of HTP and STB [22]. The helix angle, related to the HTP installation angle, determines the relationship between the pitch of the axial and transverse sections of the HTP, as follows:

$$p_{belt} = p_n = p_o \cos(\gamma) = p_t \cos(\beta), \quad 0\,\text{deg} < \gamma < 90\,\text{deg} \qquad (1)$$

where p_t is the circular pitch on the transverse section, Υ is the lead angle, which is simply calculated as $\pi/2$-β. By considering Eq. (1), it can be noted that the lead angle, Υ, of HTP must be the same as the installation angle (λ). When the installation angle becomes 90 degrees, the HTP becomes a standard timing pulley, as shown in Figure 5(b). Moreover, when it becomes 0 degrees, the HTP cannot have a helix

profile, and it is an infeasible kinematic design that cannot actuate the STB even if the HTP is rotating. The other variables in Figure 5(a) are defined as follows: t_h (Tooth height of an HTP), d (Pitch circle diameter of an HTP).

- *The condition for HTP to enable gear transmission*

Another important consideration in the design of an HTP driven by HG rotation is the necessity to ensure effective geared actuation. This can be achieved by increasing the tooth height of the HTP when compared to the tooth height of a standard timing pulley, as shown in Figure 5(c). For the HTP to be possible to be gear driven, the pitch circle (d) of the HTP must exist within the tooth profile, and the HTP pitch circle should be in point contact with the HG pitch circle. As shown in Figure 5(b), the pitch circle of a general timing pulley is located outside the tooth profile. If this tooth profile height is applied to HTP directly, the gear transmission between the HTP and the HG does not operate normally. Therefore, as shown in Figure 5(c), the HTP pitch circle must be modified to be located within the HTP tooth profile by increasing the tooth height of the HTP. In addition, according to gear theory, it is known that the depth of engagement of the teeth must be deep to increase power transmission efficiency [22]. Therefore, a design was applied to increase the height of the teeth of the HTP so that the teeth of STB and HTP can be combined, while also enabling the gear drive of HTP and HG.

- *The condition for HTP tooth array collinearity*

As shown in Figure 4(b) and Figure 5(d), the key aspect in arranging the HTP array is establishing the appropriate HTP offset (a_o) value, even as the X-axis moves, the gear connection between the HTP and STB gears is maintained, enabling independent the X-axis motion. Thus, this value should ensure the maintenance of the tooth collinear condition in reference to the HTP helical angle (β), various pitch parameters (p_o, p_t, etc.), and the HTP installation distance (a_d). As the STB moves along the X-axis, it is essential to ensure a continuous coupling condition between the tooth tread of the HTP array and the STBs. This condition is met when the tangential vector, represented as $\vec{t}^{\,w}$, of the HTP aligns with the X-axis at the position of the STB's tooth, as shown in Figure 5(d). Thus, the condition of teeth coincidence between the HTP array and STBs is represented as follows:

$$a_o = \sqrt{\left(a_d \Big/ \cos\left(\pi/2 \pm \lambda^{w}\right)\right)^2 - {a_d}^2} \tag{2}$$

where λ^w is the angle of the tangential vector of the HTP, which is calculated by $\vec{t}^{\,w}$ under the condition that the tooth of timing belt and the HTP are completely coupled in the X_w-Y_w coordinate (See Figure 5). By applying Eq. (2), the condition of continuous geared connection can be realized through the HTP tooth collinear condition.

B. Design of a HG for helical actuation of multiple HTPs

In the HTA, one HG is connected to multiple HTPs and performs geared actuation for the synchronized HTP array rotation. Thus, the helical angle and pitch design of the HG that can drive HTPs simultaneously are required, as shown in Figure 6 (See also Figure 2). To introduce a brief overview of the HG design in the X_w-Y_w coordinate system, the installation angle, θ_w, of the HG was chosen to be equal to the HTP lead angle (Υ). In Figure 6(a), an example conceptual design of the HG is presented. This constraint on the HG installation angle is established to ensure that the HG installation direction aligns with the STB installation direction, regardless of the specific values of other HTP lead angles, as shown in Figure 6(a).

To design the HG in the X_w-Y_w coordinate, the axial pitch, p_o^*, of the HG, and its helix angle (λ^*) must be defined depending on the installation angle, θ^w, of the HG. That is, for one HG to simultaneously drive multiple HTPs, the SPSG's helix angle is required as λ^*, unlike the helix angle (λ) of the HTP. The geometric alignment for geared coupling between the SPSG and the HTP necessitates the calculation of the common tangential coincidence angle (λ_{tc}^w). This angle as the key parameter for design the HG is determined by the configuration of the HTP array, as shown by the yellow straight lines in Figure 6(b). Thus, the meaning of λ_{tc}^w is the angle at which the gear teeth generated in the HG can be connected to the multiple HTPs.

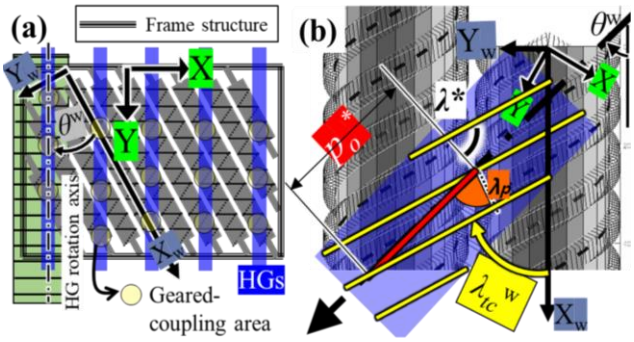

Figure 6. (a) Installation method of HG with multiple geared-coupling areas, (b) Helical angle and pitch design in the HG

To find the axial pitch, p_o^*, of the HG, a size of the HG lead angle (λ_p) can be defined by λ_{tc}^w and θ^w as follow

$$\lambda_p = \pi/2 - \lambda_{tc}^{w} + \theta^{w} \tag{3}$$

Thus, by using the HTP pitch (p) and the size of HG lead angle (λ_p), the own axial pitch, p^*, of HG is as follow

$$p^* = -p\cos\left(\pi/2 - \lambda_{tc}^{w}\right) \Big/ \left|\cos\left(\lambda_p\right)\right| \tag{4}$$

Finally, the HG helical angle, λ^* is computed as follow

$$\lambda^* = \lambda_{tc}^{w}\left(\lambda,\ a_d,\ a_o\right) + \theta^{w} \tag{5}$$

where λ, a_d, a_o are the installation angle, installation interval distance, axial offset of HTP explained in the previous section III, respectively.

IV. Motion Performance Test

A. HTA Fabrication and additional mechanisms

Based on Section III and gear kinematics theory, the final design results of HTP and HG used in the proposed ODT are computed using MATLAB, as shown in Figure 7. The detailed design and the actual fabrication of the HTA are shown in Figure 8. The design parameters of the HTP, HG, and HTA are summarized in Table I.

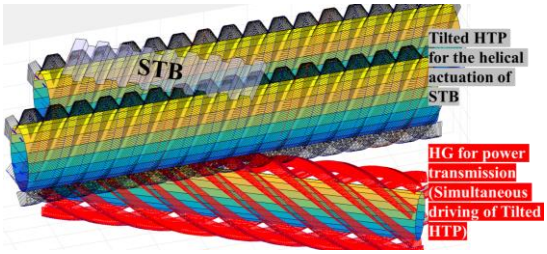

Figure 7. The final designed HTP and HG combined with STB

TABLE I. ESSENTIAL DESIGN PARAMETERS OF HG, HTP AND HTA

	Parameters	Value and note
HTP	Normal pitch (p_n)	10 mm, Same with STB pitch (STB model name: T10)
	Helical angle (β)	60 deg, lead angle :30 deg
	Number of teeth	5 threads with right hand screw type
	Tooth type	Modified tooth profile of an original timing pulley (Increased tooth height)
HG	Helical angle (λ*)	30 deg, lead angle: 60 deg
	Number of teeth	8 threads with left hand screw type
	Tooth type	Modified from standard involute profile

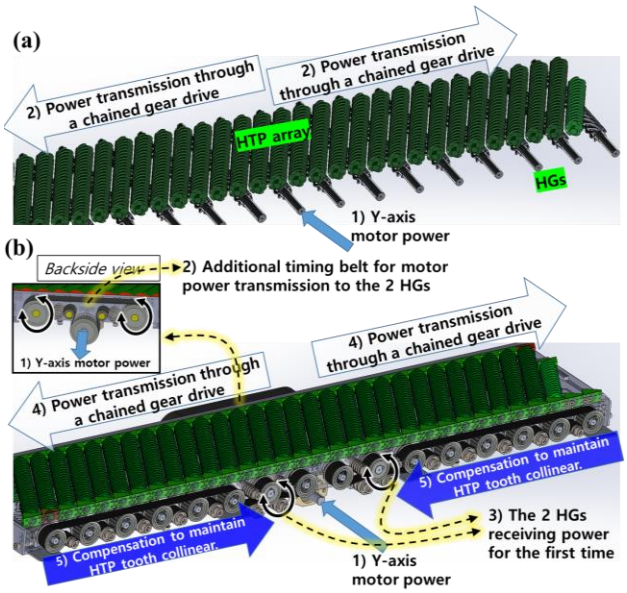

Figure 8. The final designed HTP and HG combined with STB

The main difference between the HTA detailed design in Figure 8(a) and the actual fabricated HTA in Figure 8(b) is that the HGs are combined with the additional timing pulleys. The HTA may achieve chain gear driving for all HTPs and other HGs by simply driving a single HG. However, from a practical standpoint, channeling all motor power into a single HG and relying on it to overcome all internal friction within the HTA may lead to stiffness issues. Furthermore, robustly maintaining the collinearity of HTP teeth is challenging when using chained gear driving due to the backlash between the HTP and HG.

To address the issue, extra timing pulleys and timing belts were utilized with the HGs, and the sequence of power transmission is presented to understand how the additional mechanism assisting the tooth collinearity interacts with HTPs and HGs, as shown in Figure 8(b). This additional mechanism distributes the motor's power across all HGs, reducing excessive elastic deformation of the HGs, and contributing to the effectiveness of the HTA's chained gear drive in maintaining the collinearity of the HTP teeth.

B. The proposed ODT configuration

The overall size and components of the proposed ODT are summarized in Table II. Furthermore, as shown in Figure 9, following the final assembly of the HTA, which generates Y-axis motion within the proposed ODT, it is evident that the HTP tooth alignment is properly established. The area where LI is available to respond to the user's walking measures 1.4 m x 1.4 m, which is like the length of a normal 1D treadmill.

TABLE II. THE PROPOSED ODT SPECIFICATION

Items	values
System frame size	1500 x 1500 x 240 mm
LI area and system thickness	1.4m x 1.4m x 0.24m
Unit segment size	48 x 1500 x 55 mm
Weight and total number of segments	4 kg per 1 segment, 74 units
Gear ratio of X- and Y-axis (output rotation/input rotation)	X-axis: 5/1 (increased), Y-axis: 5/8 (decreased)
Total number of HTPs and HGs	32 EA and 16 EA

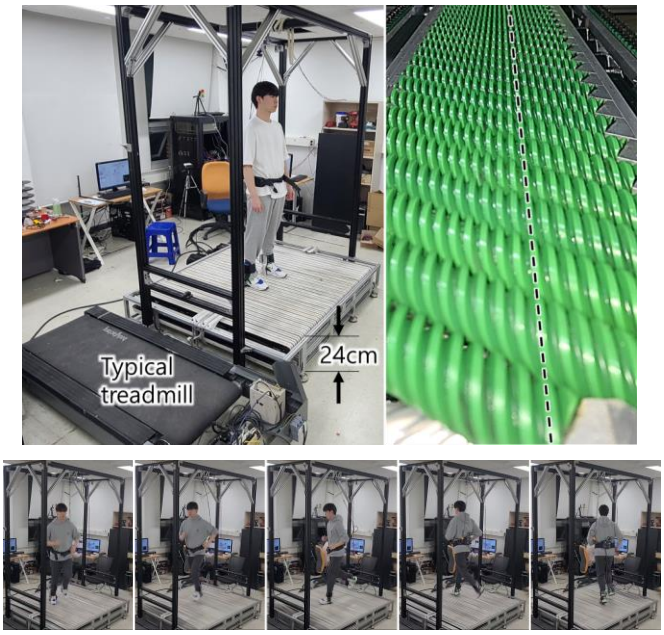

Figure 9. Overall layout of the proposed ODT with a user standing: size and thickness comparison with a typical treadmill, actual tooth collinearity state of assembled HTA, and pilot tests for running in various directions.

C. Results of Motion performance test

To measure the performance of the developed ODT, we conducted maximum acceleration and maximum velocity performance experiments. The motor speed and walking interface control are consistent with the F-ODT previously developed by the author. [21]. In the case of the X-axis, a speed of 3.175 m/s occurs when the utilized motor reaches the maximum RPM, and the Y-axis can reach 4 m/s. To assess how rapidly and stably the maximum speed can be reached for each axis, the achievable acceleration test is conducted for both axes using a sinusoidal velocity command, as follows:

$$v_c(t) = v_{\max} \sin 2\pi f, \quad \therefore a_{\max} = 2\pi v_{\max} f \tag{6}$$

where v_c is the velocity command for each axis, v_{max} is the maximum achievable velocity, and f is the input frequency of the sinusoidal signal. The test for achievable acceleration was conducted by adjusting the f value, leading to a determined acceleration of 5 m/s², which set f at 0.2 Hz for the Y-axis and 0.25 Hz for the X-axis. As shown in Figure 10, the Y-axis acceleration experiment produced satisfactory results, with the desired motion command (v_c) being effectively executed. The torque values in Figure 10(b) are presented as a ratio to the nominal torque of 69 Nm from the motor used on the Y-axis. During the execution of the sinusoidal motion command, the torque peaked at 150% of the motor's rated capacity. This higher torque requirement is due to the reduced gear ratio between the HTP (with 5 threads) and the HG (with 8 threads), which increases the rotational speed of the HTP by 1.6 times for each rotation of the HG, consequently raising the rotational resistance. However, the motor is capable of generating up to 6 times its rated torque, allowing it to handle this increased load without significant issues for periods exceeding 15 minutes.

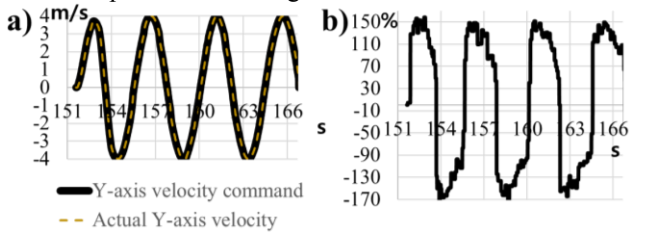

Figure 10. Verification of Y-axis motion by the motion command with 5m/s² (a) Command following performance of Y-axis to sinusoidal motion command (b) The genrated torque by the motion command with 0.2Hz

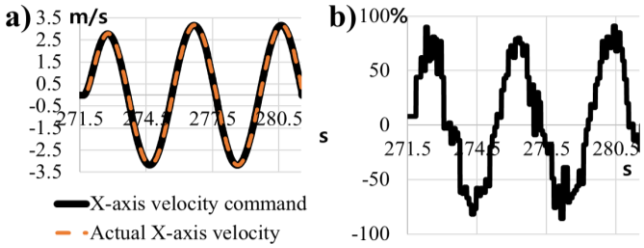

Figure 11. Verification of Y-axis motion (a) Command following performance of Y-axis to sinusoidal motion command (b) The generated torque by the motion command with 0.25Hz

The X-axis acceleration test results also show that the motion command for evaluating the acceleration performance at 5 m/s² can be performed, as shown in Figure 11(a). In the case of the generated torque results, as shown in Figure 11(b), the increased gear ratio in the X-axis allowed the desired command (v_c) to be performed within the rated torque, unlike the Y-axis motion test. Furthermore, heightened complexity in the power transmission mechanism leads to a greater demand for motor torque during motion. In contrast, the X-axis, with its simplified power transmission process, may have an advantage in reducing the required torque for motion. Finally, to attain the same maximum speed performance as the Y-axis, a reduced gear ratio should be employed.

D. Comparison to other systems

Table 3 compares the specifications of the existing ODTs and the super-thin and fast ODT proposed in this paper. The power transmission efficiency of US ARL's ODT is low when driving the segment belts. In contrast, for systems like Cyberwalk and Torus treadmill, which incorporate actuators within each segment, the added weight and complexity of the structure can restrict the performance of the X-axis. Consequently, these systems demand a high-power motor for effective operation along the X-axis. The F-ODT, a recent development by the author of this paper, and the commercially available INFINADECK exhibit relatively impressive motion performance. However, their excessive size, attributed to their bulky design, makes them impractical for use in room-scale LI setups. However, despite having a thickness similar to that of a conventional one-dimensional treadmill, the proposed ODT can generate a 2D infinite ground, and its acceleration and speed are also considered to be at the highest level.

TABLE III. COMPARISON WITH EXISTING ODTS

Existing ODTs	LI area and thickness	Actuator specification		Max. speed	Max. accel.
US ARL ODT [19]	1.3mX1.3m X 0.4m	X	4 kW(1EA)	7.2 km/h	Under 1m/s²
		Y	4 kW(1EA)		
INFINA-DECK [20]	1.2 X 1.5m X 0.4m	X	-	> 9.6km/h	-
		Y	-		-
F-ODT [21]	2.5 X 2.5m X 0.64m	X	8.8 kW(2EA)	10.9km/h 12.4km/h	3 m/s²
		Y	3.6 kW(2EA)		3 m/s²
Super-thin and Fast ODT	***1.4 X 1.4m X 0.24m***	**X**	***4.4 kW(1EA)***	***12.4km/h***	***5 m/s²***
		Y	***4.4 kW(1EA)***	***14.4km/h***	***5 m/s²***

V. CONCLUSION

In this paper, we developed a slim, high-speed omnidirectional treadmill (ODT) featuring a novel helical transmission scheme that significantly enhances acceleration and deceleration. This system incorporates a helical gear (HG) design capable of simultaneously driving all helical tooth profiles (HTPs), improving Y-axis motion with superior speed and acceleration by boosting the power transmission efficiency of the segment belt compared to traditional ODT systems. For X-axis motion, our design achieves high speed and acceleration using lighter, low-inertia segments, thanks to its simpler structure relative to existing models. Looking ahead, we aim to further enhance the immersive experience within virtual environments by simulating more complex locomotion patterns such as rapid turning, lateral walking, and backward movement. Future efforts will focus on developing an intelligent controller that builds upon the improved system performance.

ACKNOWLEDGMENT

This research was supported by the Culture, Sports and Tourism R&D Program through the Korea Creative Content Agency, funded by the Ministry of Culture, Sports and Tourism in 2023 (RS-2023-00303777), and the Translational Research Center for Rehabilitation Robots (#NRCTR-EX24008), National Rehabilitation Center, Ministry of Health and Welfare, Korea, and the AI-based GIST Research Scientist Project grant funded by the GIST in 2024 (RS-2024-00424892).

REFERENCES

[1] M. Slater and M. V. Sanchez-Vives, "Enhancing Our Lives with Immersive Virtual Reality," *Frontiers in Robotics and AI*, vol. 3, no. 74, Dec. 20INFINA16.

[2] A. Jenkins, "The fall and rise of VR: The struggle to make virtual reality get real," Fortune, https://fortune.com/longform/virtual-reality-struggle-hope-vr/ (accessed Sep. 13, 2023).

[3] K. Parrish, "VR pros still believe pricing, content is holding back mass adoption," Digital Trends, https://www.digitaltrends.com/computing/vr-pros-see-pricing-and-content-as-mainstream-barriers/ (accessed Sep. 13, 2023)

[4] J. M. Hollerbach, "Locomotion Interfaces," *Handbook of Virtual Environments: Design, Implementation, and Applications*, pp.239-254, 2002.

[5] H. Iwata, H. Yano, H. Fukushima, and H. Noma, "CirculaFloor [locomotion interface]," *IEEE Computer Graphics and Applications*, vol. 25, no. 1, pp. 64–67, 2005. doi:10.1177/0278364909104293

[6] J. Yoon, J. Park, and J. Ryu, "A planar symmetric walking cancellation algorithm for a foot—platform locomotion interface," *The International Journal of Robotics Research*, vol. 29, no. 1, pp. 39–59, 2009. doi:10.1177/0278364909104293

[7] S. Pyo, H. Lee and J. Yoon, "A Sensitive and Accurate Walking Speed Prediction Method Using Ankle Torque Estimation for a User-Driven Treadmill Interface," *IEEE Access*, vol. 10, pp. 102440-102450, 2022, doi: 10.1109/ACCESS.2022.3208352.

[8] J. Yoon, B. Novandy, C.-H. Yoon, and K.-J. Park, "A 6-DOF gait rehabilitation robot with upper and lower limb connections that allows walking velocity updates on various terrains," *IEEE/ASME Transactions on Mechatronics*, vol. 15, no. 2, pp. 201–215, 2010. doi:10.1109/tmech.2010.2040834

[9] S. H. Pyo, H. S. Lee, B. M. Phu, S. J. Park, and J. W. Yoon, "Development of an fast-omnidirectional treadmill (F-ODT) for Immersive Locomotion Interface," *2018 IEEE International Conference on Robotics and Automation (ICRA)*, 2018. doi:10.1109/icra.2018.8460669

[10] J. K. Lee, et al., "Team-based Firefighter Training Simulator for Complex Buildings," *Transactions of the Society of CAD/CAM Engineers*, vol. 16, no. 5, pp.370-379, 2011.

[11] Y. Y. Ang, P. S. Sulaiman, R.W.O. Rahmat, and N.M. Norowi. "Put down the controller, enable 'walking' in a virtual reality (VR) environment: A review." *Ambient Communications and Computer Systems*, pp. 367–379. Springer, 2018.

[12] Jiung-Yao Huang, "An omnidirectional stroll-based virtual reality interface and its application on overhead crane training," *IEEE Transactions on Multimedia*, vol. 5, no. 1, pp. 39-51, March 2003, doi: 10.1109/TMM.2003.808822.

[13] T. Cakmak and H. Hager. "Cyberith Virtualizer: A locomotion device for virtual reality." *ACM SIGGRAPH 2014 Emerging Technologies*, p. 6. ACM, 2014.

[14] Z. Wang, H. Wei, K. Zhang and L. Xie, "Real Walking in Place: HEX-CORE-PROTOTYPE Omnidirectional Treadmill," *2020 IEEE Conference on Virtual Reality and 3D User Interfaces (VR)*, Atlanta, GA, USA, 2020, pp. 382-387, doi: 10.1109/VR46266.2020.00058.

[15] Z. Wang et al., "Strolling in Room-Scale VR: Hex-Core-MK1 Omnidirectional Treadmill," *IEEE Transactions on Visualization and Computer Graphics*, 2022, doi: 10.1109/TVCG.2022.3216211.

[16] H. Taheri, B. Qiao, and N. Ghaeminezhad, "Kinematic model of a four Mecanum wheeled mobile robot," *International Journal of Computer Applications*, vol. 113, no. 3, pp. 6–9, 2015. doi:10.5120/19804-1586

[17] H. Iwata, "Walking about virtual environments on an infinite floor," *IEEE Virtual Reality (Cat. No. 99CB36316)*, Houston, TX, USA, 1999, pp. 286-293, doi: 10.1109/VR.1999.756964.

[18] M. Schwaiger, T. Thuimmel and H. Ulbrich, "Cyberwalk: An advanced prototype of a belt array platform," *2007 IEEE International Workshop on Haptic, Audio and Visual Environments and Games*, Ottawa, ON, Canada, 2007, pp. 50-55, doi: 10.1109/HAVE.2007.4371586.

[19] Angela C. Boynton, "Biomechanical and Physiological Validation of the Omni-Directional Treadmill Upgrade as a Mobility Platform for Immersive Environments", *ARMY RESEARCH LAB ABERDEEN PROVING GROUND MD*, no. ARL-TR-551, 2011.

[20] V. Metsis, K. S. Smith and D. Gobert, "Integration of virtual reality with an omnidirectional treadmill system for multi-directional balance skills intervention," *2017 International Symposium on Wearable Robotics and Rehabilitation (WeRob)*, Houston, TX, USA, 2017, pp. 1-2, doi: 10.1109/WEROB.2017.8383831.

[21] S. Pyo, H. Lee, and J. Yoon, "Development of a novel omnidirectional treadmill-based locomotion interface device with running capability," *Applied Sciences*, vol. 11, no. 9, p. 4223, 2021. doi:10.3390/app11094223

[22] F. L. Litvin and A. Fuentes, *Gear Geometry and Applied Theory*. Cambridge: Cambridge University Press, 2004.